New Aspects of Polymer Characterization by Dynamic Light Scattering**

Walther Burchard*

Can macromolecules be seen moving? No doubt, twenty years ago the answer would have been a definite «No». Today we are more inclined to answer positively, assuming we accept the observation of scattered light as a kind of seeing. The new capability of watching the motion of molecules, without exerting an external force on the system, is a typical feature of our time with its high technology in electronics and the construction of fast digital computers. Once the new technique was understood, the various aspects and possibilities were immediately anticipated by scientists. These ideas remained fairly speculative for several years, but now a stage has been reached where some of the experiments suggested earlier have since been tested and where further applications can be foreseen. Most exciting is probably the prospect of determining viscoelastic properties in some favourable cases. The present article provides an introduction to the principles of this fairly new technique. The power of the method is illustrated by two simple examples and, finally, some problems of practical interest are discussed.

Eingegangen am 23. November 1984 [FR 1]

1. Introduction

In the summer months of 1827, the British botanist *Robert Brown* was studying the shape of *Clarkia pulchella* pollen in aqueous suspension[1]. He noticed that the particles were in continuous motion and he wondered whether these organic particles were perhaps self-animated. He later corrected his speculation when he noticed the same motion also apparent with inorganic particles, but it nevertheless took a further 75 years before the movement now generally referred to as «Brownian» was indisputably accounted for in a series of five papers by *Albert Einstein*[2]. Even *Einstein*, in his first treatise, was not sure whether he was really dealing with the Brownian movement, although the French physicist and mathematician *Henry Poincare*[3] had given a correct qualitative interpretation. He observed that the Brownian motion of large

[1] Diese Tabelle mit numerischen Angaben ist entnommen aus H. Primas, U. Müller-Herold: *Elementare Quantenchemie*, Teubner Verlag, Stuttgart 1984.

[2] «The theory of resonance in chemistry ... was suggested by quantum mechanics but is no longer a branch of quantum mechanics», schreibt L. Pauling in B. Kockel, W. Macke, A. Papapetrou: *Quantum Theory and Chemistry, Max-Planck-Festschrift 1958*, VEB Deutscher Verlag der Wissenschaften, Berlin 1959, S. 385–388.

[3] Auf diesen Punkt wurde am Symposium in Emmetten insbesondere von *W. Gründler*, Halle, hingewiesen.

[4] Auf diesen Punkt wurde am Symposium in Emmetten von *L. Zülicke*, Berlin-Adlershof, hingewiesen.

* *Correspondence:* Prof. Dr. W. Burchard
Institut für Makromolekulare Chemie der Universität
Stefan-Meier-Strasse 31, D-7800 Freiburg i. Br.
(Bundesrepublik Deutschland)

** This article is based on a plenary lecture presented in September 1984 at the 8th International Macromolecular Symposium «Macromolecules – Interdisciplinary Developments» in Interlaken (Switzerland).

particles is the result of a statistical misbalance of solvent molecules knocking the particle from all sides. Since then it has been clear that the Brownian motion is a statistical problem.

Einstein's study led him to some very important conclusions which, because of their relevance, should be mentioned here in some detail. He considered the escape of n particles out of a small volume element in x-direction, where on average these particles have a velocity v (See Fig. 1 for illustration). The change in concentration within the volume element, caused by this escape, is connected with a decrease in the osmotic pressure π with x, and the osmotic force $-\partial\pi/\partial x$ must in thermodynamic equilibrium be balanced by the frictional force nfv, where f is the frictional coefficient of the particles. Now, $nv = j$ is the flux of particles, and the force balance

$$nfv = -\partial\pi/\partial x \tag{1}$$

leads to a relationship for the flux

$$j = nv = -(1/f)\partial\pi/\partial x = -(kT/f)\mathrm{d}n/\mathrm{d}x \tag{2}$$

where van't Hoff's law for the osmotic pressure of an ideal solution ($\pi = kTn$) is used. Equation (2) has the form of the first Fick law of diffusion, which leads to the conclusion

$$D = kT/f = kT/(6\pi\eta_0 R_h) \tag{3}$$

which is now known as the Stokes-Einstein relationship. The relationship between the frictional coefficient and the radius of a sphere was already established in Stokes' [4] outline of hydrodynamics. The second equivalence in equation (3) will be taken as a definition for a hydrodynamically effective radius even for particles which do not show spherical symmetry.

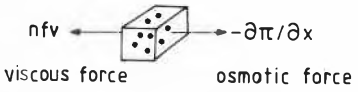

Fig. 1. Sketch for the osmotic force and the frictional force (viscous force) as result of a density fluctuation due to Brownian motion. n: number of Brownian particles, π: osmotic pressure, v: average velocity of a particle, and f: frictional coefficient.

From the point on when *Einstein* arrived at his famous relationship, scientists eagerly began looking for techniques to measure the Brownian motion. Such facility was finally found with the technique of dynamic light scattering; however, not before the development of lasers as sources of extreme monochromacy could this technique be implemented.

2. Line Width and Time Correlation Function

The basic idea of dynamic light scattering is simple and not at all new. It results from the well-known Doppler effect[5] according to which the frequency of a moving transmitting source is shifted to higher or lower frequencies if the source is moving towards or away from a detector. The shift is proportional to the ratio of the speed of the source, v_0, to the wave propagation velocity, c. Molecules in gases and solution move in all directions in space and show a speed distribution. Therefore a continuous broadening of the line, rather than a discrete shift, is observed. The line width broadening is proportional to the translational diffusion coefficient[6]. Unfortunately, the motion of larger molecules in a viscous medium is slowed down appreciably, too much, in fact, as to display a significant line width broadening which could be resolved with even the best Fabry-Perot spectrometers[7].

A way out of this dilemma was found by the British group associated with *Pike* from the Royal Radar and Signals Establishment[8], who remembered the Wiener-Khintchine[9,10] theorem. According to this theorem a well behaved function $C(t)$ exists in the time domain which is adjoined to the power spectrum $S(\omega)$ of a line in the frequency domain. Both functions are pairs of a Fourier transform with respect of time and frequency.

$$S(\omega) = (2\pi)^{-1}\int_{-\infty}^{+\infty} C(t)\mathrm{e}^{i(\omega t)}\mathrm{d}t \tag{4}$$

$$C(t) = \int_{-\infty}^{+\infty} S(\omega)\mathrm{e}^{-i(\omega t)}\mathrm{d}\omega \tag{5}$$

The value of the Wiener-Khintchine theorem becomes evident if a constant value of ωt is considered. If ω is so small as to be undetectable by spectroscopy, a large time interval exists associated to this line width broadening which is often large enough to allow computations by special fast computers. Fig. 2 shows the corresponding regions in the frequency and time domains.

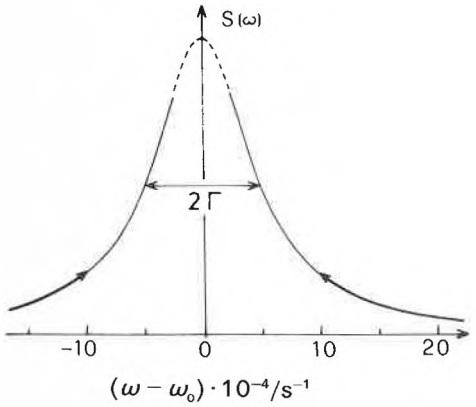

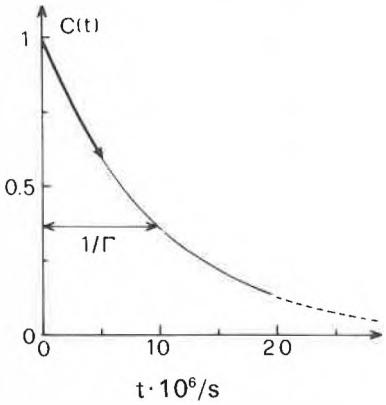

Fig. 2. Shape, $S(\omega)$, of a spectral line that is broadened by the Doppler effect (above), and corresponding time correlation function, $C(t)$, in the time domain (below). The line width Γ is proportional to the translational diffusion coefficient. $S(\omega)$ and $C(t)$ are related to each other through a Fourier transform, given by equations (4) and (5). The corresponding regions of ωt = const. in the frequency and time domains are indicated by the same curve symbols.

3. Time Correlation Function of the Scattering Intensity

The slow motion of macromolecules makes it necessary to work in the time

Walther Burchard: Born on May 15, 1930 in Poznan (Poland). Training in Physics at the Universities of Marburg an der Lahn and Freiburg im Breisgau. Since 1957 at the Institute of Macromolecular Chemistry, University of Freiburg. There he received his Ph.D. (Physics) and Habilitation (Physical Chemistry of Polymers). Professor since 1972. Research interests: Solution properties of biological and synthetic macromolecules. Main interest is directed to water soluble polymers and to investigations of branched structures (structure of anylopectin, fibrin formation, microgels, thermoreversible gels, heterogeneous networks). Development of a suitable branching theory for interpretation of light scattering data. Since 1977 work on dynamic light scattering (experimental and theoretical).

domain and to learn how to handle the data. In conventional light scattering (LS), a large scattering volume and a long time of recording is chosen. Under such circumstances all fluctuations resulting from the motion of the molecules are averaged out. In dynamic LS the scattering volume is made small and the time of recording short, i.e. of the order of 1μs or even shorter. Then the scattering intensity shows strong fluctuations as shown schematically in Fig. 3.

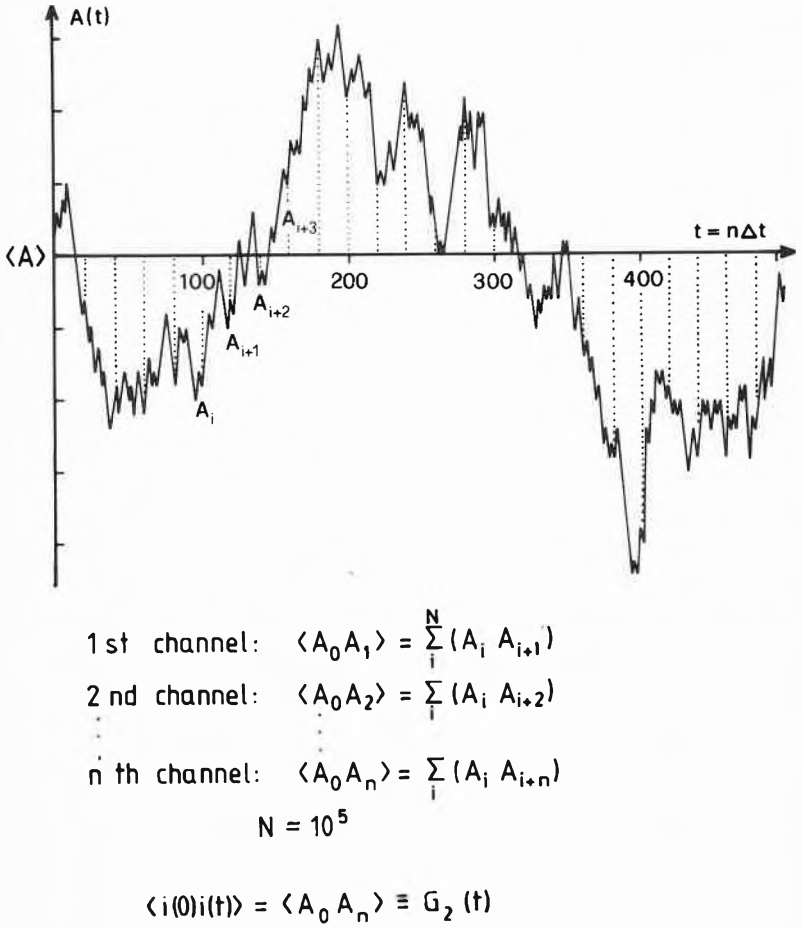

Fig. 3. Short time scattering intensity fluctuations around the mean ⟨A⟩ which represents the static light scattering intensity. A_i is the number of photons arriving at the detector in a time interval $\Delta t \approx 10^{-6}$ s; N is the number of products $A_i A_{i+n}$ formed by the number of photons in the i-th time interval and in the time interval $n\Delta t$ later.

These fluctuations do not result from a variation in the number of molecules in the scattering volume but are caused by incidental clustering of molecules[11], which gives rise to a strong scattering intensity, followed by a dissociation, whereupon only little light is scattered.

Thus these fluctuations contain information on the mobility of the macromolecules which can be extracted as follows. Let A_i be the number of photons arriven at the detector in the time interval Δt. By means of a fast computer the number of photons from two successive time intervals are multiplied, and the product is stored in a first channel of the correlator. This procedure is repeated about 100000 times and stored in channel 1. In channel 2 the products of photon numbers A_i and A_{i+2} are stored etc, and eventually in the last channel n the products of A_i and A_{i+n} are collected. The result of this manipulation is shown in Fig. 4a for a poly(methyl methacrylate) (PMMA) sample of low polydispersity in acetone. The exponentially decaying function is called the time correlation function (TCF) of the scattering intensity. This name is easily understood if we recall that the time interval chosen for the recording of photons was very small; hence most of the molecules have not yet collided with others. They thus have a good memory of the direction and magnitude of their velocities during the time interval just past. However, after a longer delay time the molecules will have suffered many collisions and will have lost all memory of their initial velocity. Thus the curves in Fig. 4 describe the decay from a highly correlated to a fully uncorrelated motion. One notices from Fig. 3 that fluctuations occur around an average which is the scattering intensity that is recorded by static LS[11].

4. Properties of the Time Correlation Function

The recorded TCF of the scattered light is, in general, not simply related to the motion of the molecules. In most cases, however, the following approximation renders a sufficient accuracy

$$< i(0)i(t) > = A + |g_1^2(t)| = G_2(t) \qquad (6)$$

$$g_1(t) = \frac{< |E^*(0)E(t)| >}{< E^*(0)E(0) >} = \frac{S(t,q)}{S(q)} \qquad (7)$$

$$\text{with } q = (4\pi/\lambda)\sin\theta/2 \qquad (8)$$

$g_1(t)$ is the normalized TCF of the scattered electric field. The denominator in equation (7) will be recognized as the static structure factor $S(q)$, and $S(q,t)$ is the dynamic structure factor.

For monodisperse particles small in diameter compared to the wavelength of the light and also for hard monodisperse spheres of any size, $g_1(t)$ is easily calculated and is a single exponential

$$g_1(t) = \exp(-\Gamma t) = \exp(-Dq^2 t) \qquad (9)$$

In most cases, however, the decay of $g_1(t)$ is more complex, and the TCF shows a more slowly decaying tail. Such a tail can be seen already with the fairly homogeneous poly(methyl methacrylate) sample as shown in Fig. 4b. Such behaviour may result either from polydispersity or from internal modes of motion. Both effects may be demonstrated with two highly simplified examples.

5. Polydispersity

Let us assume that the system contains only two species of molecules of different size. Then the TCF consists of the sum of two exponentials

$$g_1(t) = a(q)\exp[-D_1(q^2 t)] + b(q)\exp[-D_2(q^2 t)] \qquad (10)$$

where D_1 and D_2 are the diffusion coefficients of the two particles. The coefficients $a(q)$ and $b(q)$ are the corresponding amplitudes for the two particles which in general depend on the scattering angle. They are related to the particle scattering factors of the static light scattering. The decay constants in $g_1(t)$ depend on the delay time but also on the scattering angle. According to equation (10) it is sometimes advisable to use the parameter $q^2 t$ as the variable for the abscissa, since then the two steps of the relaxation occur for measurements at different scattering angles at the same position.

6. Internal Modes of Motion

A flexible or soft particle will perform a number of internal modes of motion. These motions result in local segment density fluctuations and give rise to additional contributions to the TCF with a characteristic time which corresponds to

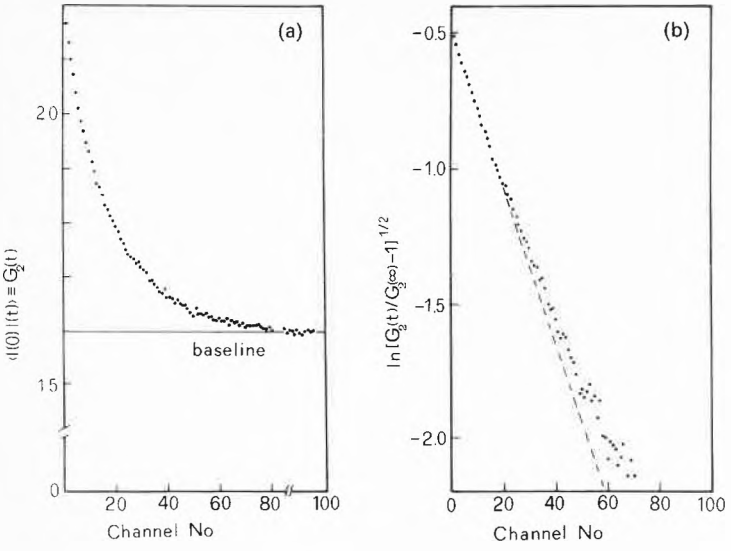

Fig. 4. (a) Scattering intensity time correlation function $G_2(t) = \langle i(0)i(t) \rangle$ of a poly-(methyl methacrylate) (PMMA) sample in acetone as function of the delay time, and (b) the corresponding electric field time correlation function $g_1(t)$, here, however, plotted as In $g_1(t)$ versus time t. The PMMA sample had a poldispersity of $M_w/M_n = 1.14$; still deviations from a single exponential are observed at large delay times.

Fig. 7 shows the TCF's of such microgels at various scattering angles where a reduced delay time $\hat{t} = t[\sin^2(\theta/2)/\sin^2(45°)]$ was used. For hard monodisperse spheres the measurements at different angles should form one common TCF which is a single exponential with the translational diffusion coefficient as decay constant. The microgels exhibit different behaviour. Only at low angles is, as expected, a single exponential observed, but with increasing scattering angle the TCF's sag more and more and show a faster initial decay. With large delay times all curves run parallel to each other. This common asymptote is easily recognized as the effect of the translational diffusion of the center of mass of the particles. The initial faster decay, which gains weight with increasing scattering angle, corresponds to the appearance of a faster relaxation process.

Evidently the situation here is that of equation (11), and the faster relaxation may be interpreted as the influence of the slowest internal mode of motion, which may be a breathing mode.

the relaxation time superimposed to the translational motion. Again, the simplest case may be considered here, where only the longest internal motion contributes to the TCF with a sufficient amplitude. Then $g_1(t)$ is given by[11,12]

$$g_1(t) = a(q) \exp[-D(q^2t)] + b(q) \exp[-(D + 1/\tau_1 q^2)(q^2t)] \quad (11)$$

where τ_1 is the relaxation time of the internal motion which, as a characteristic parameter of the molecule, cannot depend on the scattering angle. Therefore, in a plot of $g_1(t)$ against q^2t only the diffusive process will occur at the same value of the abscissa if measurements at different angles are plotted in the same graph, while the second process will show a shift to smaller values of q^2t with an increasing scattering angle.

These oversimplified cases will now be illustrated by observations made during two experiments.

7. Microgels[13,14]

Many dynamic LS measurements have been performed with latex particles which are the best examples of monodisperse hard spheres. Here, however, the behaviour of microgels will be discussed. These microgels were prepared by emulsion polymerization of butylmethacrylate with the addition of a small amount of butyldivinyl ether [14]. After a certain monomer conversion, crosslinking occurred within the latex particle. When the surrounding soap was removed the material could be dissolved in organic solvents where the microgel swelled appreciably under maintenance of the spherical shape. A sketch of this crosslinking reaction is shown in Fig. 5, and electronmicrographs from the latex particles and the material obtained after removal of the surrounding soap are seen in Fig. 6.

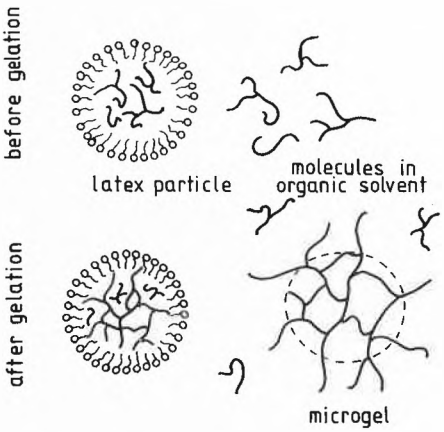

Fig. 5. Crosslinking reaction within latex particles. At low monomer conversion small and only slightly branched molecules are obtained; the reaction is random since the molecules do not feel the boundaries of the encapsuling soap layer. With increasing conversion the molecules grow in size and molecular weight until some of these reach a structure which spans all over the available space in the latex particle. At further conversion the molecules no longer can grow in size (radius of gyration); intramolecular reactions (network formation) occur but further monomers can be added to the gel fraction. The spherical shape becomes conserved. After removal of the soap the material becomes readily soluble in organic solvents. At low conversion, i.e. before gelation, randomly branched molecules are found, after gelation swollen microgel particles are observed together with smaller molecules which belong to the sol fraction.

8. Semidilute Solutions

In the second example the change of mobility of linear poly(vinylpyrrolidone) (PVP) molecules on increasing the polymer concentration was studied. Before turning to the results, however, it will be useful to recall what types of motion can be expected[15,16].

(a) In dilute solution (see Fig. 8) the molecules are isolated, and only one translational motion will be observed, which is influenced by hydrodynamic and thermodynamic interaction with the surrounding other coils. The concentration dependence can be described by[17,18]

$$D_z = (M_w/N_A f_c)(\partial\pi/\partial c) \quad (12)$$

where π is the osmotic pressure and f_c the concentration-dependent friction coefficient.

(b) At higher concentrations the coils start to overlap; they interpenetrate each other and form an entangled network. A reliable estimate for the overlap concentration is[15,19]

$$c^* \approx 1/[\eta] \quad (13)$$

This concentration is used now by *de Gennes* as a scaling factor, and all properties of the entangled network are expressed in terms of c/c^*.

De Gennes predicts two types of motion. The first one is related to the elastic modulus which is determined by the correlation length ξ (Fig. 9); this is the length between two points of entanglement. The irregular motion of these chain sections can be represented by a cooperative diffusion coefficient, which in the scaling theory is given by[15]

$$D_{coop} \approx kT/(6\pi\eta_0\xi) \approx (c/c^*)^{0.75} \quad (14)$$

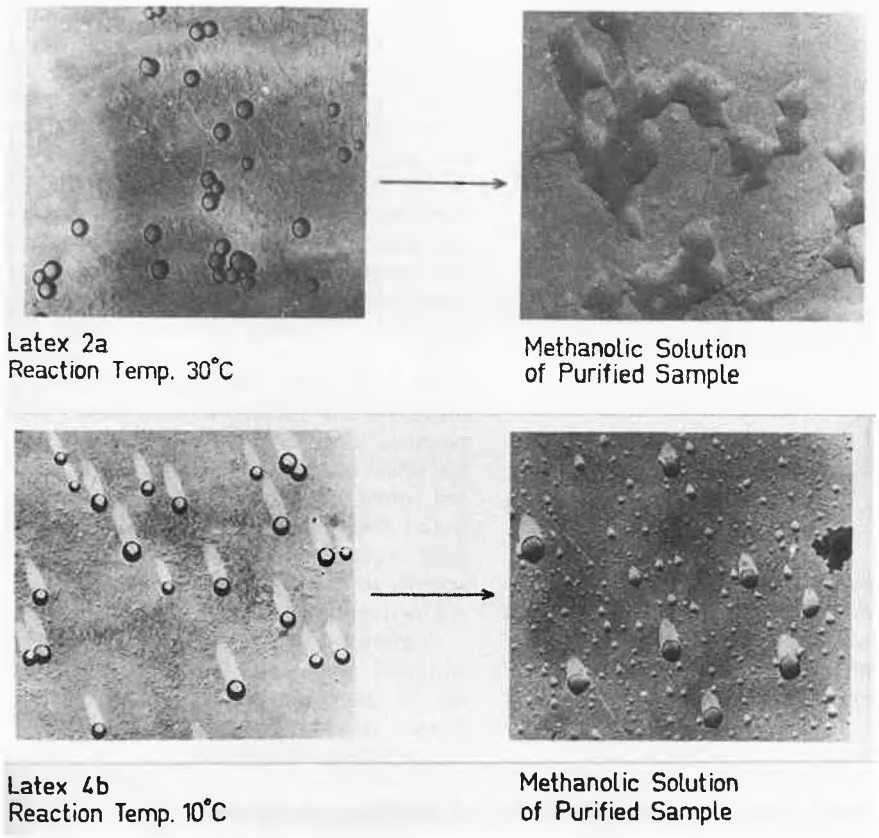

Fig. 6. Electron micrographs of latex particles obtained by emulsion polymerization of poly(vinyl acetate) (PVAc) (left side) and of the corresponding particles in methanol after removing the soap, above: before gelation, below: after gelation. The swollen microgels and the small molecules of the sol fraction are clearly seen.

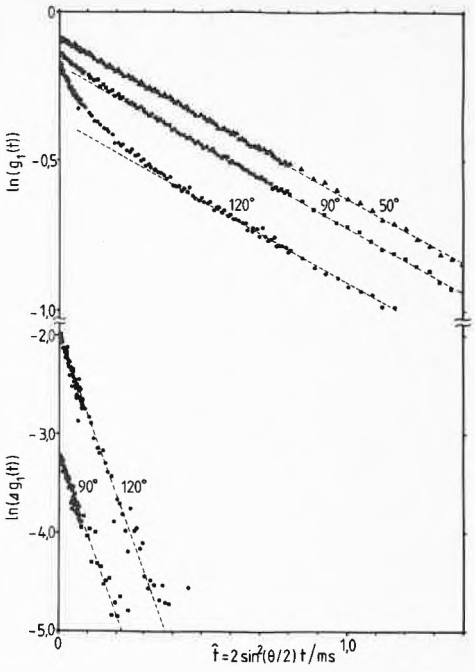

Fig. 7. Time correlation functions of PVAc microgels at three scattering angles. A reduced time $\hat{t} = t[q^2(\theta)/q^2(90°)]$ was chosen where $q(0) = (4\pi/\lambda)\sin\theta/2$, with λ the wavelength in the solution and θ the scattering angle. The slope of the parallel lines at larger delay times gives the translational diffusion coefficient of the centre of mass; the faster decay at short delay times and larger scattering angles result from internal modes of motion. The curve in the lower part of the figure shows the difference between the experimental curve and the single exponential at large delay times[14].

Of course, with increasing concentration the correlation length becomes shorter and the motion faster.

The second type of motion is a self-diffusion where the chains in the entangled system move along their own contour length (Fig. 10). The motion is slowed down remarkably with increasing chain length and concentration. *De Gennes* predicts[16]

$$D_{self} \approx N^{-2} c^{-1.75} \qquad (15)$$

We carried out dynamic and static light scattering measurements from poly(vinylpyrrolidone) (PVP) in aqueous solution[20]. PVP is a nonionic vinylpolymer with a lactam ring as side group. Fig. 11 shows five TCF's from two concentrations below c^* and three above[21, 22]. A logarithmic time scale was used since the motions slowed down drastically. A single exponential decay assumes, in this plot, a sigmoidal shape, and such behaviour is indeed observed with the two lower concentrations. Above c^*, however, a second much slower process becomes apparent and quickly gains weight. With our old correlator the TCF's had to be spliced together, but recently we acquired a correlator which allows the recording of such widely spread correlation functions in one run[23]. Fig. 12 gives an example.

Next, it was necessary to check whether the processes were diffusive or internal relaxations, Fig. 13 shows three TCF's of one concentration at various angles but now plotted against q^2t[21, 23]. The two decaying processes occur here at the same positions which, according to equation (10), is indicative of diffusive motions. Fig. 14 shows the concentration dependence of D_{fast} and D_{slow} which apparently do not follow exactly *de Gennes'* prediction.

For the determination of the two diffusion coefficients in equation (10) *Provencher*[24] developed a special program, CONTIN, which allows, besides the diffusion coefficients, evaluation of the amplitude factors $a(q)$ and $b(q)$. These in general depend on the scattering angle and have to be extrapolated to zero angle i.e. $q \rightarrow 0$. In Fig. 15, $w_{slow} \equiv b$ $(q = 0)$ is plotted against the reduced concentration c/c^*, yielding an approximately straight line with an exponent as indicated in the figure. This curve can tentatively be extrapolated towards 100% slow mode, which would be around $c = 10c^*$. One may wonder what this point means.

A hint may be taken from the simultaneously recorded static LS, which enabled determination of the radius of gyration of the polymer at that concentration. One notices from Fig. 16 that this radius remains almost constant until c^* is reached; then a drastic increase is observed. Similar behaviour was observed many years ago by *Dautzenberg*[25] with polystyrene in benzene, although the effect in those days was disregarded. In context with the dynamic measurements, the increase of $\langle S^2 \rangle$ appears in a different light. Evidently, beyond c^* entangled clusters are formed which grow in size resulting in a drastic slow-down of the translational motion. Thus, just beyond c^* we are not in a gel but still in the pre-gel state, and the concentration where $w_{slow} = 1$ can be regarded as the gel point[26, 27]. This conclusion is of relevance since only beyond this concentration the scaling law by *de Gennes* can be expected to hold. Experiments to prove this conjecture are underway.

The other two curves in Fig. 14 will not be discussed here. (For more details see[21, 22]). The present outline should be sufficiently clear to indicate the exciting new possibilities in the study of semidilute solutions.

9. Molecular Weight Distribution

Obviously the simple cases discussed so far are very rare. In most systems a full size distribution is present, and in large

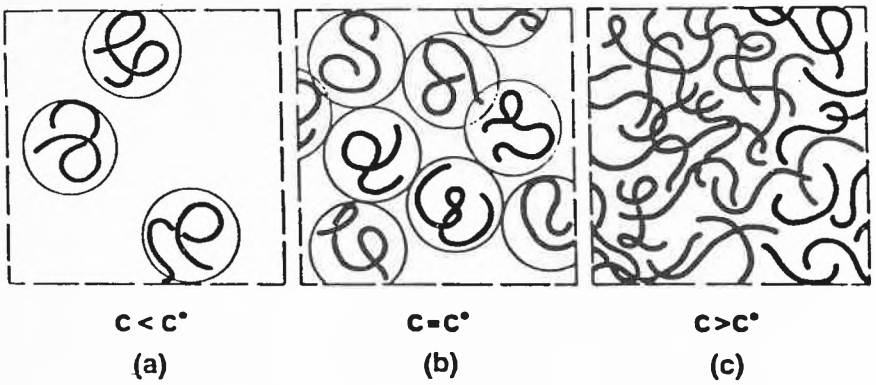

Fig. 8. Polymers in solution at different concentrations. $c^* \approx 1/[\eta]$ is the coil overlap concentration. Solutions with $c < c^*$ are dilute, those with $c > c^*$ semidilute. For large molecular weights the concentration in this highly entangled stage is still low (≈ 2%)[16].

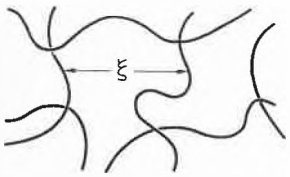

Fig. 9. Enlarged section from Figure 8c. ξ is the correlation length. The cooperative diffusion (representing a «breathing» of the gel) is inversely proportional to the correlation length[16].

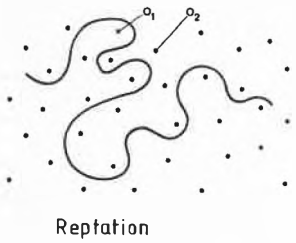

Fig. 10. A single chain in a network of entangled chains. Only motion along the contour length is possible, for which de Gennes coined the expression «reptation» in remembrence of the motion of a reptile[16].

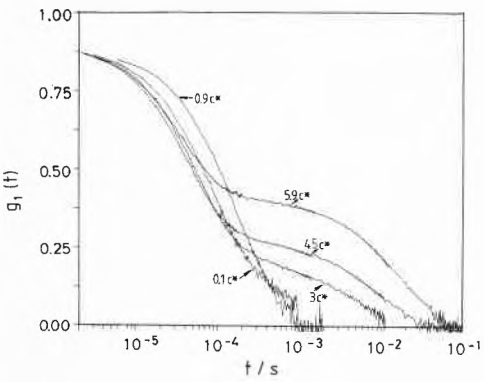

Fig. 11. Time correlation functions of a poly(vinyl pyrrolidone) (PVP), M_w = 560000, at five concentrations at 90°C. Note: $g_1(t)$ is plotted here against log t. Four time correlation functions, recorded with different sample times, had to be spliced together when a conventional correlator was used[21,22].

macromolecules also a spectrum of various overtones of relaxation modes. If we confine ourselves to molecules which show no angular dependence of the scattered light, the internal modes are not detectable, and the shape of the time correlation function is solely determined by the molecular weight distribution and is given by

$$g_1(t) = \frac{\int w(M) M \exp(-D(M)q^2 t)\,dM}{\int w(M) M\,dM} \quad (16)$$

where $w(M)$ is the weight fraction of polymers of molecular weight M. The molecular weight dependence of the diffusion coefficient $D(M)$ can, over a wide range, be represented by a simple exponential relationship

$$D(M) = KM^{-\nu} \quad (17)$$

where for linear chains ν lies between 0.5 and 0.59, depending on the solvent used. Hence the shape of $g_1(t)$ is given as

$$g_1(t) = \int w(M) M \exp(-KM^{-\nu} q^2 t)\,dM/M_w \quad (18)$$

which in principle can be solved for the distribution $w(M)$.

The actual solution of the integral equation is a mathematically complex problem because of the always existent noise that is superimposed to an ideal, smooth TCF. Recently *Provencher*[24] developed the already mentioned program CONTIN which enables evaluation of $w(M)$ to a very satisfactory precision. Fig. 17 shows as an example the time correlation function of a poly(2-trimethylammoniomethyl methacrylate)chloride (PTMAC) sample of M_w = 110000, and Fig. 18 charts the distribution[28] obtained from the analysis of $g_1(t)$ in Fig. 17.

This aspect of determining molecular weight distributions from dynamic light scattering is certainly animating and will be tested in the next years thoroughly in various laboratories. The technique has on the other hand limitations, since for larger molecules the spectrum of internal relaxation modes contribute to $g_1(t)$, and in many cases a general analysis in terms of polydispersity and relaxation modes ceases to be feasible.

10. Cumulant expansion and First Cumulant

Valuable information about the system can be obtained, however, by studying the TCF at fairly short delay times and, on the other hand, at large q-values. The short time behaviour will be discussed first.

The initial part of a correlation function can in most cases be approximated by a single exponential, and it is therefore sensible to try a cumulant expansion, where the logarithmic TCF[29,30] is expanded in a power series in terms of the delay time t.

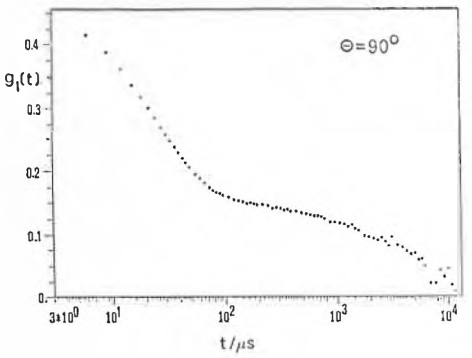

Fig. 12. Time correlation function of the same PVP as shown in Fig. 11 at $c = 10c^*$ recorded by a correlator with logarithmic spacing of the delay times[23]. *Both relaxation processes could be measured now within one run.*

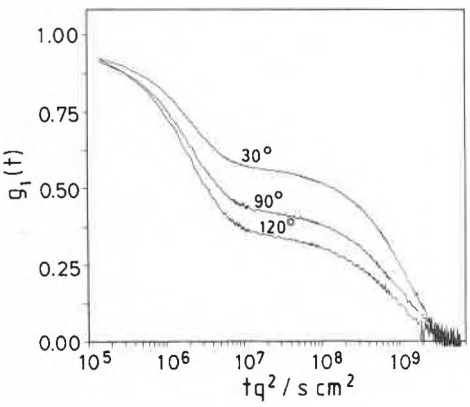

Fig. 13. Three time correlation functions at different scattering angles for the same PVP as shown in Fig. 11, but now plotted as function of q^2t. The two relaxation processes appear here at the same abscissa values which indicates the diffusive character[21,22].

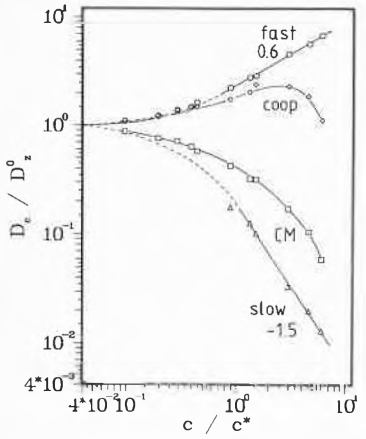

Fig. 14. Concentration dependence of the fast and slow modes of motion. The numbers indicate the exponents ε in $D/D_o \sim (c/c^*)^{\varepsilon}$. Both exponents are smaller in value than predicted by de Gennes for an entangled network[21,22].

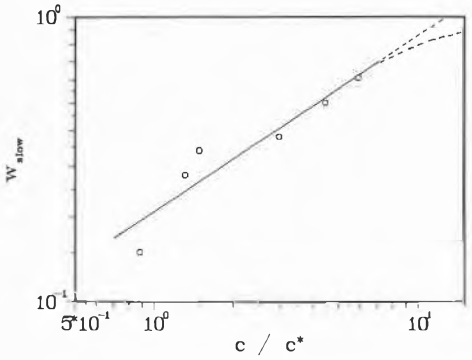

Fig. 15. Increase of the slow mode amplitude $w_{slow} \equiv b(q = 0)$ with the polymer concentration. Around $c = 10c^*$ the amplitude w_{slow} approaches 1, which may indicate a gel point. At lower concentrations clusters of entangled chains appear to be present (pre-gel state)[21,22].

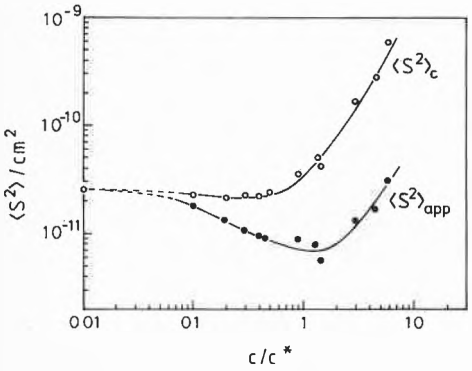

Fig. 16. Concentration dependence of the apparent and true mean square radius of gyration of the same PVP sample as in Fig. 11 to 15. $\langle S^2\rangle_{app}$ is obtained directly from a Zimm plot, and the true radius of gyration is obtained from the relationship $\langle S^2\rangle_z = \langle S^2\rangle_{app}(M_w/M_{app})$, where M_{app} is given by equation (23)[21,22].

$$\ln g_1(t) = -\Gamma_1 t + (\Gamma_2/2!)t^2 - (\Gamma_3/3!)t^3 + \ldots \quad (19)$$

where Γ_1, Γ_2, etc are the first, second, etc cumulants.

Most interesting is the first cumulant since it can be calculated by equilibrium statistical thermodynamics[31]. One result is that the first cumulant can be expressed at low q^2 as follows[32]

$$\Gamma = D_c q^2(1 + C\langle S^2\rangle q^2) \quad (20)$$

with

$$D = D_c(1 + k_D c + \ldots) \quad (21)$$

where D_c is the diffusion coefficient at a finite concentration, $\langle S^2\rangle$ the mean square radius of gyration and C a coefficient which is characteristic for the molecular architecture. For hard spheres, for example, $C = 0$; for a random coil, C is 0.2 and branching causes a decrease. Also chain stiffness has an influence on C which was studied recently by *Stockmayer* and *Schmidt*[33].

It is interesting to compare the relationship for the reduced first cumulant Γ/q^2 with that of Debye's equation for the static light scattering, which shows a striking formal similarity.

$$Kc/R_\theta = (1 + 1/3\langle S^2\rangle q^2)/M_{app}(c) \quad (22)$$

with

$$1/M_{app}(c) = (1 + 2A_2 M_w c + \ldots) \quad (23)$$

Static LS measurements are commonly evaluated from Zimm plots; consequently the first cumulant may be analysed from a corresponding *dynamic* Zimm plot. Fig. 19 shows these two types of Zimm plots for a polystyrene sample of $M_w = 2.88 \cdot 10^6$ [34]. With our instruments we are able to measure static and the dynamic light scattering simultaneously. Thus six quantities have been obtained from these two Zimm plots which are listed in Table 1[22].

Table 1. The six quantities which are obtained from static and dynamic Zimm plots.

	intercept	slopes c = 0	q = 0
static LS	M_w	$\langle S^2\rangle_z$	A_2
dynamic LS	D_z	$C\langle S^2\rangle_z$	k_D

These quantities can be combined, and three such combinations lead to new parameters which are characteristic for the architecture of the molecule. The one is the coefficient C which has been already discussed. Another one is the coefficient k_{fo} which is obtained from the data of A_2, k_D and the hydrodynamic volume v_h[35–38]

$$k_{fo} v_h (N_A/M_w) = 2A_2 M_w - k_D - v_2 \quad (24)$$

with v_2 the partial specific volume of the polymer in solution.

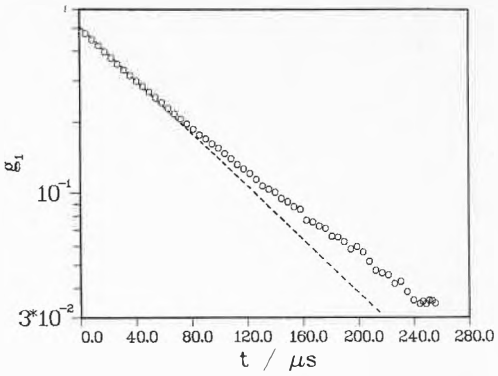

Fig. 17. Time correlation function $g_1(t)$ of a poly(2-trimethylammoniomethyl methacrylate)chloride (PTMAC) in 1 N NaCl aqueous solution ($M_w = 110000$)[28].

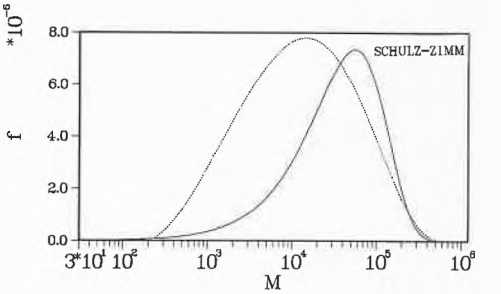

Fig. 18. Molecular weight distribution obtained from $g_1(t)$ in Fig. 17[28] *using the program CONTIN by Provencher*[24]. *For comparison the Schulz-Zimm distribution of the same polydispersity is shown.*

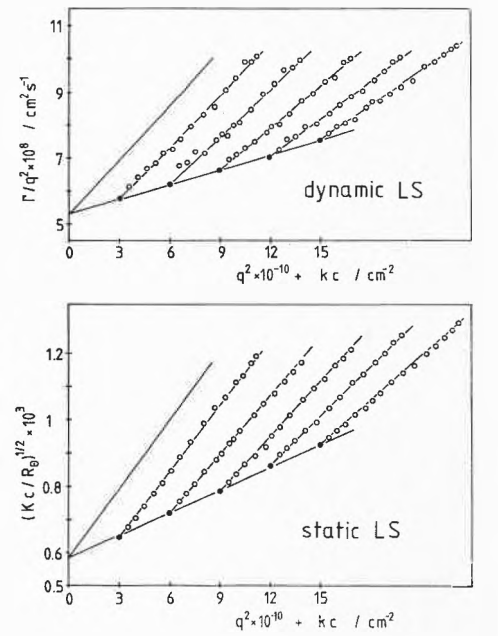

Fig. 19. Static and dynamic Zimm plots from a polystyrene sample ($M_w = 2.88 \cdot 10^6$). Six quantities, listed in Table 1, can be obtained from such simultaneous static and dynamic light scattering measurements[20].

This coefficient is a measure of the coil interpenetration of two molecules in a good solvent at very high dilution.

Most instructive is the third parameter[31]

$$\rho = R_g/R_h \qquad (25)$$

where $R_g \equiv \langle S^2 \rangle^{1/2}$ is the radius of gyration and R_h the hydrodynamically effective radius which is defined by the Stokes-Einstein relationship

$$D = kT/(6\pi\eta_0 R_h) \qquad (3)$$

The hydrodynamic radius has in the limit of large molecular weights the same dependence on the bond length and the degree of polymerization as the radius of gyration, but it is still not identical. R_h depends on (in addition to the geometric dimensions) the hydrodynamic interaction. For instance in a branched molecule the segment density is higher than in a linear chain of the same radius of gyration. As a consequence, the solvent becomes to a larger extent be immobilized than in a linear chain, and this results in a larger hydrodynamic radius or a smaller value for the parameter ρ. A decrease of ρ, which is even stronger than predicted by theory, has been indeed observed with star branched molecules with 4, 6, 8, 12 and 18 arms[39].

Most striking is the effect on ρ for the microgels[13]. Fig. 20 shows the results of measurement of $\langle S^2 \rangle$ and D for PVAc that was polymerized in emulsion to various monomer conversions. The measurements were made in methanol after the soap had been removed. Up to a molecular weight of about 10^7 both the radius of gyration and the molecular weight increase; this is typical for a random branching process. However, when a molecular weight of about 10^7 is passed, the radius of gyration remains essentially constant or may even decrease slightly. Similarly, D remains constant. Evidently, the molecules have reached here a size so as to span across the entire space of the latex particle; the molecule can grow in weight but no longer in dimension because of the boundary of the encapsuling soap. In other words, at $M_w \approx (10\text{–}20) \cdot 10^6$ gel formation takes place. Fig. 21 shows the change of the ρ-parameter in the course of reaction, and now a marked transition from the structure of randomly branched molecules to values even lower than for a hard sphere is observed, allowing a precise determination of the gel point in this finite system.

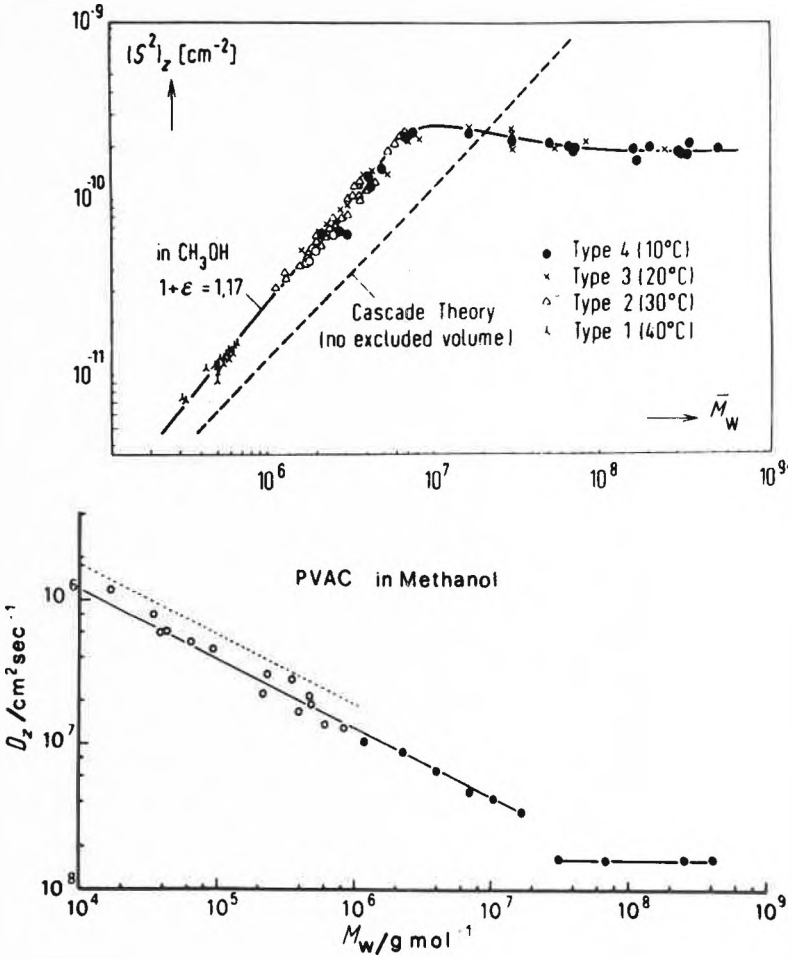

Fig. 20. Change of $\langle S^2 \rangle_z$ and D_z with molecular weight M_w for poly(vinyl acetate) (PVAc) in methanol polymerized in emulsion[13].

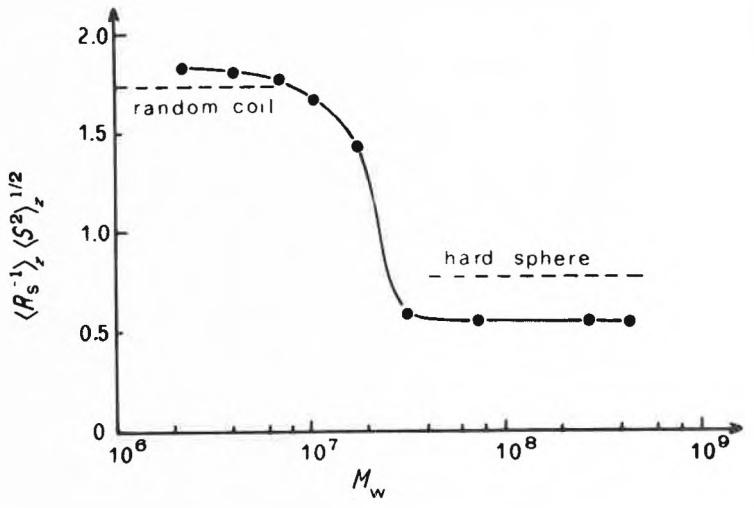

Fig. 21. Variation of the parameter $\rho \equiv \langle S^2 \rangle^{1/2}/R_h$ with molecular weight for the same PVAc samples as shown in Fig. 20.

11. Asymptotic Behaviour

Another limiting behaviour of the time correlation function is observed for large macromolecules at large values of the scattering vector q. Here the shape of the time correlation function becomes fully independent of the size or the molecular weight of the molecules[40]. This behaviour is presently the center of much discussion, and the question as to what influence branching and crosslinking have on this shape is under investigation[41]. The subject will not be discussed here further for lack of theoretical explanation.

12. Gels and Networks

This short survey can be concluded with some remarks on gels and networks. Three types are distinguishable, i.e. (1) permanent gels formed by covalent bonds, (2) thermoreversible gels, where junction zones form physical crosslinks which can «melt» on heating, and (3) the transient network of entangled chains (pseudogels).

The permanent gels and the transient networks of entangled chains will be discussed first. Such comparison is possible since the entangled chains can be cross-

linked, for instance by γ-ray irridiation. Following the scaling arguments as outlined by *de Gennes*, scientists did not expect a difference, but recent measurement by *Munch* et al.[42, 43] revealed about 10% higher cooperative diffusion coefficients for permanently crosslinked polystyrene gels than for the corresponding pseudogels.

The interpretation given by *Candau* et al.[43] is based on the theory of motion in an isotropic elastic body by *Tanaka* et al.[44, 45]. Accordingly, the cooperative diffusion is given by

$$D_{coop} = (K + (3/4)G)/\rho f \qquad (26)$$

where $K = c\,\partial\pi/\partial c$ is the osmotic compressibility (or bulk modulus in the melt) and G is the shear modulus; ρ is the mass density and f the frictional coefficient.

The interesting part in this continuum theory is the shear modulus appearing in equation (26), which commonly is measured by mechanical devices, i.e. rheometers. Here now a possibility of determining G by dynamic light scattering emerges. Estimation of the magnitude of K and G in solutions of a few per cent reveals, however, that the osmotic compressibility is the leading term, and precision measurement of the osmotic compressibility by other techniques, e.g. by static light scattering, is needed before G can be compared with that obtained from mechanical measurements. The higher diffusion coefficient in real gels compared to those in pseudogels is interpreted as being due to differences in the shear modulus. This conjecture needs, however, to be tested more comprehensively.

The theory of dynamics of an isotropic elastic body does not predict a slow mode which is observed in pseudogels. All measurements with real gels seem to indicate that the slow mode disappears when the gel point is passed[45, 46]. It is now interesting that the slow mode remains in thermoreversible networks. Fig. 22 gives an example with the potassium salt form of

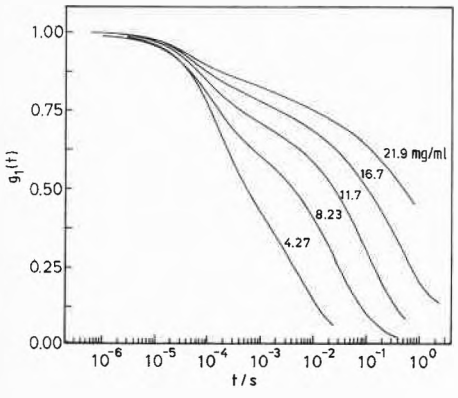

Fig. 22. Time correlation function for iota-carrageenan at 15.6 °C and five concentrations[47]. *Note that the delay time is plotted here in a logarithmic scale.*

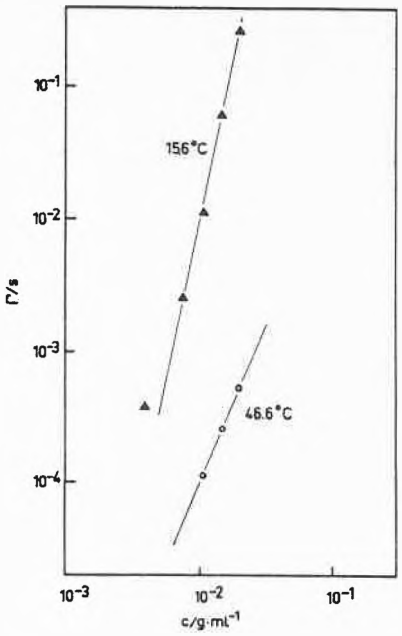

Fig. 23. Concentration dependence of the mean relaxation time $\langle\tau\rangle \sim 1/D_{slow}$ *for iota-carrageenan at 15.6 °C and 46.6 °C. The numbers indicate the exponents in equation (27)*[47].

iota-carrageenan at five concentrations[47, 48]. Further information was obtained when the mean relaxation time $\langle\tau\rangle \sim 1/D_{slow}$ was plotted against the concentration in a double logarithmic scale (Fig. 23). Exponents of $\varepsilon = 4.80$ and 2.43 in the equation

$$D_{slow} \approx c^{-\varepsilon} \qquad (27)$$

were found at 15.5 °C (gel) and 46.6 °C (solution), respectively. The value for the solution is fairly close to 1.75 for repeating linear chains, but the exponent of 4.8 in the gel state describes a much stronger decrease in mobility. These findings can tentatively be explained by a breaking of junction zones, which in carrageenan form the crosslinks, and these opened bonds may form shortly thereafter new junction zones with other parts of the gel. On the whole an apparent translational diffusion will result by this breaking and forming of bonds in a thermodynamic equilibrium[47, 48].

Received: November 26, 1984 [FR2]

[1] R. Brown, *Philos. Mag. 4* (1827) 294.
[2] A. Einstein, *Ann. Phys. (Leipzig) 17* (1905) 549; *19* (1906) 289, 371; *Z. Elektrochem. 13* (1907) 41; *14* (1908) 235.
[3] H. Poincare, paper delivered at the Congress of Arts and Science in St. Louis (France) 1904.
[4] G.G. Stokes, *Trans. Cambridge Philos. Soc. 8* (1847) 287; *9* (1851) 8.
[5] C. Doppler, *Abh. Königl. Böhm. Ges. Wiss. 2* (1842) 465.
[6] M. Born; *Optik*, Springer-Verlag, Berlin 1965.
[7] C. Fabry, H. Buisson, *C.R. Acad. Sci. 154* (1912) 1224, 1500.
[8] E. Jakeman, C.H. Oliver, E.R. Pike, *J. Phys. Chem. A1* (1968) 406.
[9] N. Wiener, *Acta Math. 55* (1930) 117.
[10] A.J. Khinchine, *Math. Ann. 109* (1934) 604.
[11] B. Berne, R. Pecora: *Dynamic Light Scattering*, Wiley, New York 1976.
[12] R. Pecora, *J. Chem. Phys. 40* (1964) 1604.
[13] M. Schmidt, D. Nerger, W. Burchard, *Polymer 20* (1979) 582; *Ber. Bunsenges. Phys. Chem. 83* (1979) 388.
[14] D. Kunz, A. Thurn, W. Burchard, *Colloid Polym. Sci. 261* (1983) 635.
[15] P.-G. de Gennes, *Nature (London) 282* (1979) 367.
[16] P.-G. de Gennes: *Scaling Concepts in Polymer Physics*, Cornell University Press, Ithaca, NY 1979.
[17] S. DeGroot, P. Mazur: *Thermodynamics of Irreversible Processes*, North Holland, Amsterdam 1952.
[18] H. Yamakawa: *Modern Theory of Polymer Solutions*, Harper and Row, New York 1971.
[19] H.L. Frisch, R. Simha in F.R. Eirich: *Rheology*, Academic Press, New York 1956.
[20] S. Bantle, M. Schmidt, W. Burchard, *Macromolecules 15* (1982) 1604.
[21] M. Eisele, W. Burchard, *Macromolecules 17* (1984) 1636.
[22] M. Eisele, W. Burchard, *Pure Appl. Chem. 56* (1984) 1379.
[23] ALV-3000 Correlator/Structurator, supplied by ALV Langen/Hessen (Federal Republic of Germany).
[24] S.W. Provencher, *Biophys. J. 16* (1976) 27; see also E.O. Schulz-Dubois: *Photon Correlation Techniques in Fluid Mechanics*, Springer-Verlag, Berlin 1983.
[25] H. Dauzenberg, *Faserforsch. Textiltech. 21* (1970) 341.
[26] P.J. Flory: *Principles of Polymer Chemistry*, Cornell University Press, Ithaca, NY 1953.
[27] H.H. Stockmayer, *J. Chem. Phys. 11* (1943) 45; *12* (1944) 125.
[28] H. Schlager, W. Burchard, to be published.
[29] D. E. Koppel, *J. Chem. Phys. 57* (1972) 4814.
[30] P. Pusey in: *Photon Correlation Spectroscopy*, Plenum Press, New York 1973, p. 387.
[31] A.Z. Akcasu, H. Gurol, *J. Polym. Sci. Polym. Phys. Ed. 14* (1976) 1.
[32] a) W. Burchard, M. Schmidt, W.H. Stockmayer, *Macromolecules 13* (1980) 1265; b) W. Burchard, *Adv. Polym. Sci. 48* (1983) 1.
[33] M. Schmidt, W.H. Stockmayer, *Macromolecules 17* (1984) 509.
[34] S. Bantle, M. Schmidt, W. Burchard, *Macromolecules 15* (1982) 1604.
[35] H. Yamakawa, *J. Chem. Phys. 36* (1962) 2995.
[36] C.W. Pyun, M. Fixamn, *J. Chem. Phys. 41* (1964) 937.
[37] S. Imai, *J. Chem. Phys. 50* (1969) 2110.
[38] A.Z. Akcasu, M. Benmouna, *Macromolecules 11* (1978) 1193.
[39] K. Huber, W. Burchard, L.J. Fetters, *Macromolecules 17* (1984) 541.
[40] A.Z. Akcasu, M. Benmouna, C.C. Han, *Polymer 21* (1980) 866.
[41] W. Burchard, A. Thurn, Int. Workshop on Plant Polysaccharides, Structure and Function, INRA, Nantes 1984, p. 31.
[42] J.P. Munch et al., *J. Phys. (Paris) 38* (1977) 971, 1499.
[43] S.J. Candau, J. Bastide, M. Delsanti, *Adv. Polym. Sci. 44* (1982) 27.
[44] T. Tanaka, L. Hocker, G.B. Benedek, *J. Chem. Phys. 59* (1973) 515.
[45] L. Landau, E. Lifschitz: *Theory of Elasticity*, Pergamon Press, London 1970.
[46] S.J. Candau, M. Ankrim, J.P. Munch, G. Hild, *Br. Polymer J.* (1985), in print.
[47] H.-U. ter Meer, *Ph. D. Thesis*, Universität Freiburg 1984.
[48] W. Burchard, *Br. Polymer J.* (1985), in print.